Publication V

DYNAMIC STRAIN AGING OF NI-BASE ALLOYS INCONEL 600 AND 690

H. Hänninen[1], M. Ivanchenko[1], Y. Yagodzinskyy[1], V. Nevdacha[1], U. Ehrnstén[2], P. Aaltonen[2]

[1] Helsinki University of Technology, Department of Mechanical Engineering, Puumiehenkuja 3, P.O. Box 4200, FIN-02015 HUT, Finland
[2] VTT Technical Research Centre of Finland, Industrial Systems, Kemistintie 3, P.O. Box 1704, FIN-02044 VTT, Finland

Abstract

Dynamic strain aging (DSA) and jerky flow phenomena in the commercial Ni-base alloys Inconel 600 and 690 have been investigated. Tensile tests were performed in the strain rate range of 10^{-3} to 10^{-6} s^{-1} at temperatures of 100 – 600 ^{o}C. No remarkable difference in the DSA behaviour of Inconel 600 and 690 alloys was observed. Tensile properties of the studied alloys in the DSA temperature range, and type and characteristics of jerky flow were obtained and analysed. The map for occurrence of serrated flow as a function of strain rate and temperature was built for Inconel 600 and 690 alloys and the activation enthalpies of dynamic strain aging appearance were found to be 1.6 eV for both materials. The obtained enthalpy of DSA appearance corresponds well to the enthalpy of carbon diffusion (1.76 eV), which was estimated by means of internal friction for the studied Inconel 600 alloy. The mechanisms of DSA based on interstitial atom interactions with dislocations in the studied alloys are discussed and the results are analysed based on the susceptibility of these alloys to environmentally assisted cracking (EAC).

Introduction

The occurrence of dynamic strain aging (DSA) has been extensively studied in many engineering alloys, which are applied in the nuclear power industry [1 - 7]. Recently quite much attention is paid to austenitic stainless steels and especially AISI 316L steel [8 - 12]. There are only a few studies published on this phenomenon in Inconel alloys which play an important role in the nuclear power industry [13 - 18].

DSA occurs in alloys containing solute atoms which can rapidly and strongly segregate to dislocations during straining. This phenomenon leads to an inhomogeneous plastic flow or serrated yielding during straining at elevated temperatures and results often in a remarkable degradation of mechanical properties. In different materials various solute atoms and a number of mechanisms can participate in the solute atom – mobile dislocation interactions. For instance, in austenitic stainless steels carbon and nitrogen interstitials or interstitial-vacancy pairs and at higher temperatures substitutional solute atoms such as Cr and Mo can interact with dislocations and be the cause of the appearance of DSA serrations [8 - 12]. In nickel-base alloys and superalloys interstitial (H and C) and substitutional (Cr) solute atoms are usually responsible for jerky flow [13 - 18].

Mulford and Kocks have found that DSA phenomenon takes place in Inconel 600 alloy over a wide range of temperature and strain rate [13]. Interstitials play a key role in DSA of pure Ni which has been shown for Ni-C and Ni-H interstitial alloys [14]. In Ni-C alloys the lower critical temperature of DSA occurrence had an activation enthalpy of about half of that for bulk diffusion of carbon and it was associated with carbon diffusion in the dislocation core. Additionally it was observed that serrations were not affected by quenched-in vacancies [15]. Temperature of DSA occurrence in Inconel 600 alloy was found to be close to that of austenitic stainless steel and markedly higher than that of Ni-C binary alloy [15]. Based on this result it was concluded that C-Cr and N-Cr complexes may also play an important role in the DSA mechanism.

Alloy 600 is used as material, e.g., for vessel head penetrations in pressurized water reactors (PWR). Primary water stress corrosion cracking (PWSCC) as well as intergranular stress corrosion cracking (IGSCC) in components other than steam generators are the problems of intensive research for nuclear power plants. Role of EAC mechanisms related to crack tip plastic deformation in the highly deformed material of the plastic zone is the key question of this study.

Aim of the present investigation was to study the DSA phenomenon in Inconel 600 and 690 alloys and its effects on their mechanical properties. By means of internal friction (IF) technique the investigation of DSA mechanism of Inconel alloys was extended to interstitial atom diffusion.

Experimental methods

Two commercial Ni-base alloys Inconel 600 and Inconel 690 were studied. Chemical compositions of the materials are shown in Table 1.

A series of uniaxial tensile tests was conducted in the laboratory air under axial displacement control with constant cross-head speeds corresponding to initial strain rates of 1×10^{-3}, 1×10^{-4}, 1×10^{-5} and 1×10^{-6} s^{-1}. The tests were carried out over a range of temperatures from ambient up to 700 ^{0}C. All tests were performed in laboratory air.

Table I. Chemical compositions of the studied alloys in weight %.													
	Ni	Cr	Fe	Cu	Al	Co	Nb	Ti	C	Si	Mn	S	P
Inconel 600	rest	16.1	8.1	0.01	0.17	0.29	0.01	0.16	0.04	0.32	0.22	<0.01	<0.01
Inconel 690	rest	27.7	8.4	0.01	0.18	0.07	0.01	0.14	0.01	0.23	0.22	<0.01	<0.01

A 25 kN MTS 858 testing machine was used in the tensile tests. A split-design furnace with temperature control of accuracy of ±1 °C was used for tests at elevated temperatures. A high temperature extensometer (gauge length of 12 mm) was used to measure strain. Tensile test specimens were prepared according to ASTM standard E 8M (sheet-type sub-size specimens). Tensile tests were performed according to ASTM standard E21 (Standard Test Method for Elevated Temperature Tension Tests of Metallic Materials).

Materials were supplied as two metal plates in mill-annealed condition with thickness of about 14 mm for Inconel 600 and 5 mm for Inconel 690. Average grain size of the studied alloys was about 100 µm for Inconel 600 alloy and about 30 µm for Inconel 690 alloy. Materials were cut using water-jet cutting and spark-erosion techniques to form the flat specimens. The specimen surface was polished using SiC emery paper down to 800 grit to remove surface defects and to obtain dimensions of 1.9 × 6 × 32 mm.

Base materials, materials in pre-strained condition and some specimens quenched after the tensile test were studied using the internal friction (IF) technique. The specimens used for IF measurements after tensile testing at elevated temperature were strained to fracture and then quenched in water from the test temperature to room temperature within less than 1.5 min. The tensile test specimens were prepared with slight reduction in cross-section area (about 2 %) in one end of the gauge length in such a way that enough material for IF specimens was available.

The IF specimens after tensile testing with typical sizes of about 0.5 × 2 × 35 mm were cut from the gauge length parts of the tensile test specimens by an abrasive disc-saw. IF specimens for studying the as-supplied condition were cut in the tensile test direction. All IF specimens were polished with 1200 grit emery paper to avoid surface effects.

Temperature dependencies of internal friction Q^{-1} and natural frequency of the pendulum were measured in the temperature range from room temperature to 600 °C. The amplitude of the deformation in the torsion pendulum did not exceed 10^{-5} and the natural frequency of the pendulum was changing in the range of 0.5–3.0 Hz. Heating rate of the specimens during IF measurements was kept at 2 °C/min.

Results

Constant elongation rate tensile (CERT) tests were conducted in order to obtain the map of DSA serration appearance depending on strain rate and temperature for commercial grade Inconel 600 and 690 alloys. The effect of DSA on mechanical properties of the studied alloys is also investigated. Typical engineering stress-strain curves obtained at the strain rate of 10^{-5} s^{-1} are shown in Figs. 1 a and b.
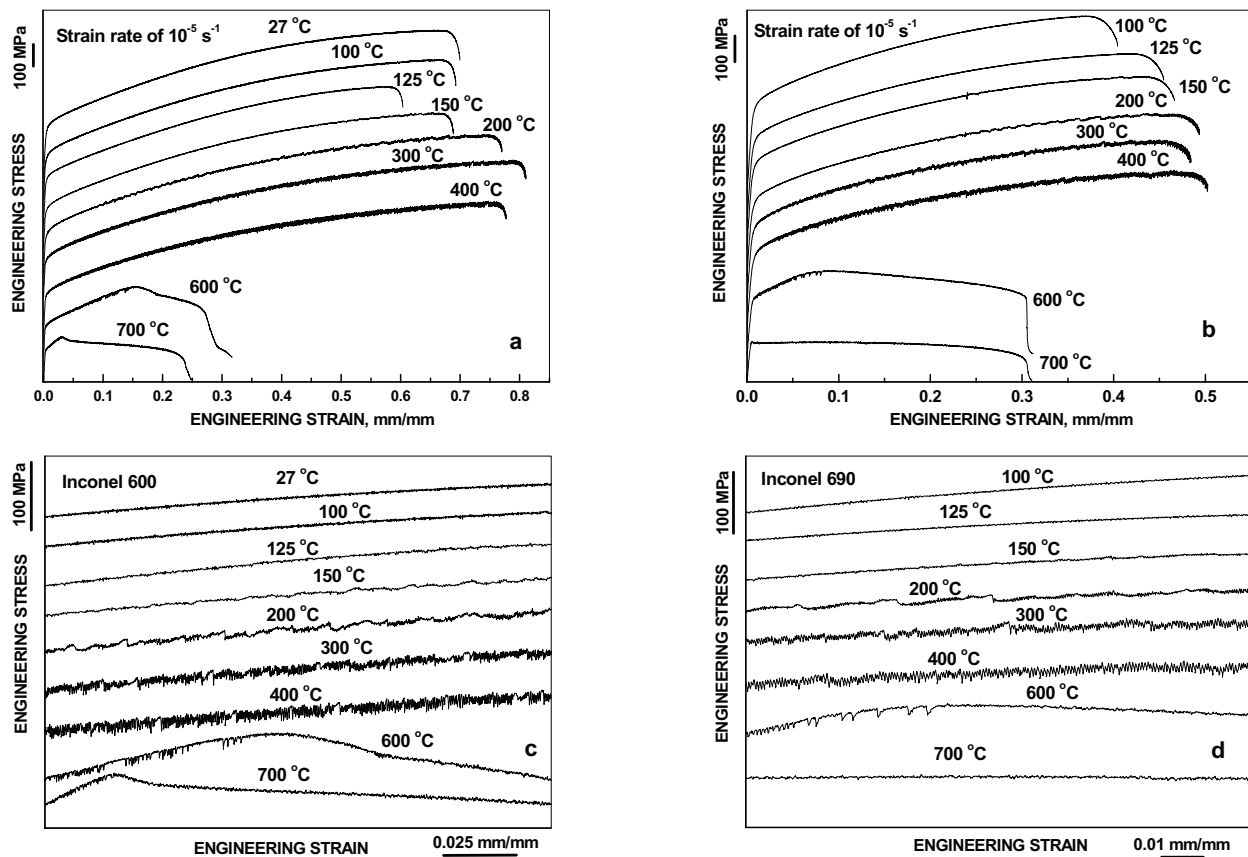

Figure 1. Engineering stress-strain curves obtained at the strain rate of 10^{-5} s^{-1} for Inconel 600 alloy (a and c) and for Inconel 690 alloy (b and d). (c) and (d) present magnified parts of the engineering stress-strain curves showing serration appearance.

DSA serrations are observed in both Inconel alloys in the range of temperatures. It can be seen from Figs. 1 c and d that at strain rate of 10^{-5} s^{-1} the DSA range extends from 150 to 600 $^{\circ}$C.

Mechanical properties

The results of DSA manifestation in mechanical properties are presented in Fig. 2. Yield stress and ultimate tensile stress decrease with increasing testing temperature up to 200 $^{\circ}$C and remain constant after that, Figs. 2 a and b. The strain hardening coefficient increases with increasing testing temperature up to 200 $^{\circ}$C, while it is almost constant above 200 $^{\circ}$C for both studied alloys, Fig. 2 c. As a function of temperature, the elongation to fracture increases for both Inconel alloys except for alloy 600 at 400 $^{\circ}$C a decrease of ductility is observed, Fig. 2 d.

Evolution of DSA serrations with temperature

Three types of serrations can be seen depending on the testing temperature in both Inconel alloys, Figs. 1 c and d. At 150 $^{\circ}$C

DSA serrations appear only on the stress-strain curves just before the specimen fracture as weak pulses related to type A serrations. At 200 $^{\circ}$C serrations are seen as well-defined pulses of type A, which appeared after certain amount of strain. At 300 $^{\circ}$C jerky flow is described by A+B type serrations appearing immediately when the plastic flow takes place. Only B type serrations are observed at 400 $^{\circ}$C in both Inconel alloys. At 600 $^{\circ}$C jerky flow appears just after yield point and the serrations can be recognized as type C serrations. All three types of jerky flow have been observed previously and are well described for other Ni-base alloys as well [13-18].

Fourier spectra of DSA serrations observed in the stress-strain curves of Inconel 600 and 690 alloys tested at the strain rate of 10^{-5} s^{-1} in the temperature range of 100 to 400 $^{\circ}$C are shown in Figs. 3 a and b, respectively. It can be seen that at 100 $^{\circ}$C the Fourier spectrum of the flow stress signal represents only random noise. In the presence of quasi-regular serrations of type A on the stress-strain curve at 200 $^{\circ}$C low frequency maxima shown by
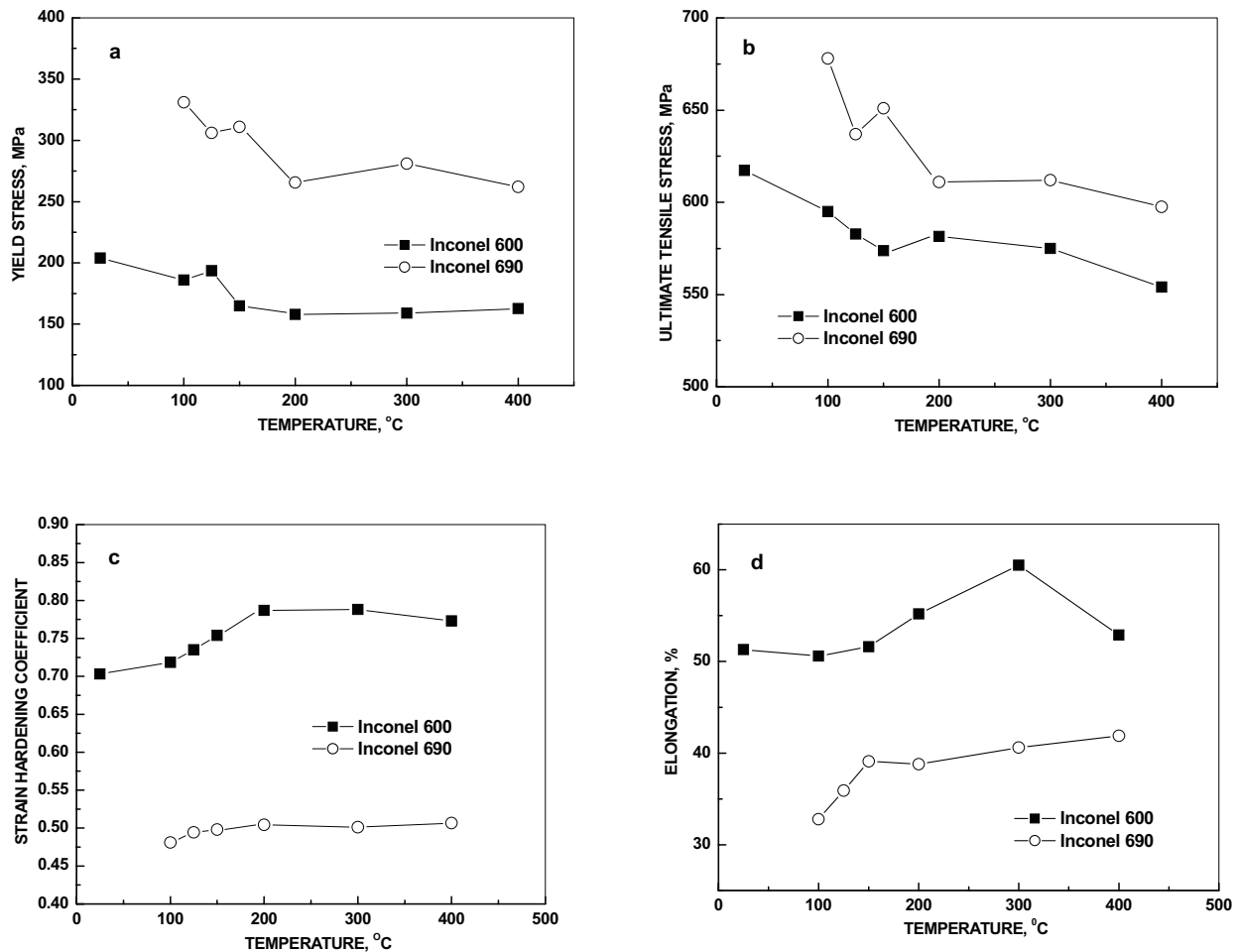

Figure 2. Temperature dependence of yield stress (a), ultimate tensile stress (b), strain hardening coefficient (c) and elongation to fracture (d) of the studied Inconel 600 and 690 alloys.
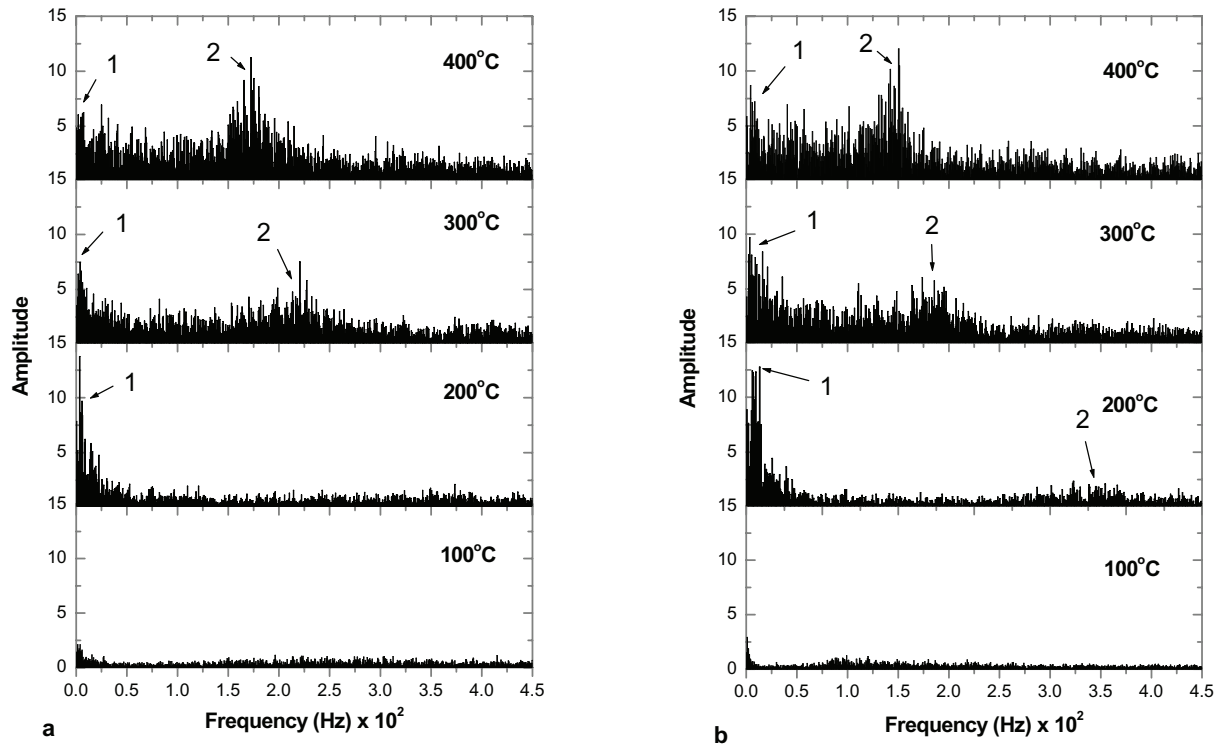
Figure 3. Fourier transformation spectra of the flow stress signal in the tensile tests of Inconel 600 (a) and 690 (b) alloys at the strain rate of 10^{-5} s^{-1} and different temperatures; 1 corresponds to low frequency maxima and 2 to high frequency maxima.

arrows and marked as 1 in Fig. 3 arise in the Fourier spectra of both Inconel alloys. Application of the Gaussian distribution to maxima in the low frequency part of Fourier spectra gives a modal value of frequency around 5.5×10^{-4} Hz for Inconel 600 alloy and 6.0×10^{-4} Hz for Inconel 690 alloy corresponding approximately to 1.8 ks and 1.7 ks, respectively. These two characteristic times reflect repeated advancement of the Lüders band through the specimen. It can be seen that amplitudes of A type serrations decrease with temperature, when high frequency maxima arise in the Fourier spectra, which are marked as 2 in Fig. 3 and correspond to type B serrations.

Internal friction

Internal friction (IF) of the studied Inconel alloys was mainly measured to check the presence of free interstitial carbon atoms in the crystal lattice of the studied alloys. Typical temperature dependencies of IF obtained for Inconel 600 and 690 alloys in the as-supplied state are presented in Fig. 4.

The IF peak with temperature position around 350 °C is present on the IF curve of Alloy 600 in as-supplied state and represents Snoek-like relaxation process due to elemental diffusion jumps of interstitial carbon atoms in FCC crystal lattice of the alloy. This peak is attributed to relaxation process and in Arrhenius coordinates it follows a linear dependency, Fig. 5. The activation energy of the IF peak was calculated and its value is about 1.76 eV. Amplitude of the IF peak increases with the amount of cold deformation. The height of the IF peak increases even more after

tensile tests at elevated temperatures and especially when the DSA serrations have been present, Figs. 6 a and b.

The IF peak in the deformed Alloy 600 is not stable and its amplitude decreases at testing temperature with annealing time. Effect of annealing at 347 °C for 7 h on the height of the IF peak of the specimen after CERT testing at 300 °C within DSA range is presented in Fig. 7 a. Dependence of the IF value on the aging time is plotted in Fig. 7 b and it can be described by two decreasing exponents with the characteristic times of about 1.5 ks and 21.9 ks.

Carbon Snoek-like IF peak is seen only in Inconel 600 alloy and it was not detected in Inconel 690 alloy at all. The IF peak was neither detected in Inconel 690 alloy after cold deformation (16.6 %) nor in specimens after CERT testing at 200 and 300 °C within the DSA range. The IF peak was neither found in another heat of Inconel 690 alloy with 0.02 wt. % C. The absence of the carbon peak in Inconel 690 alloy is probably caused by a specific distribution of interstitial atoms with higher chromium content of this alloy composition. Almost two times higher Cr content in Inconel 690 alloy in comparison to Inconel 600 alloy decreases the carbon solubility due to $M_{23}C_6$ type chromium carbides. The higher Cr content results also in an increase of interstitial octahedral positions with 6 Cr atoms at the vertices of octahedron, which do not take part in the carbon IF peak due to their cubic symmetry [19].
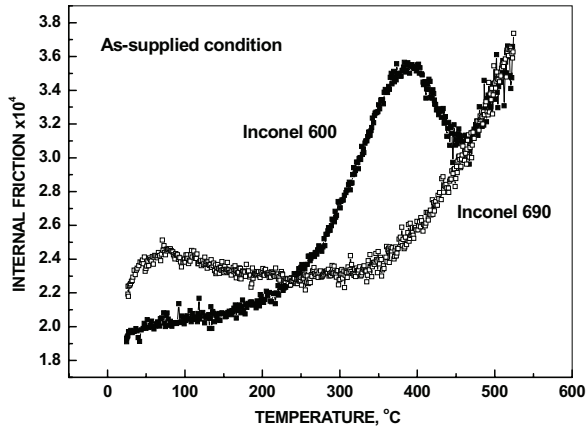
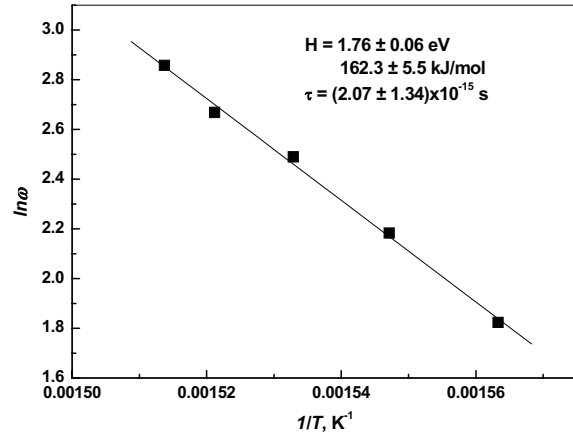Figure 4. IF of Inconel 600 and 690 alloys in as-supplied state.

Figure 5. Activation parameters of the carbon IF peak in Inconel 600 alloy.
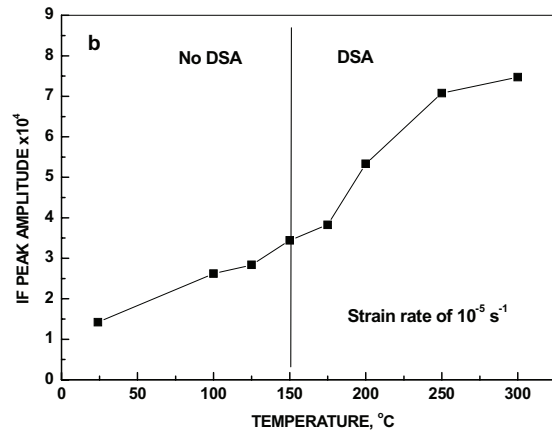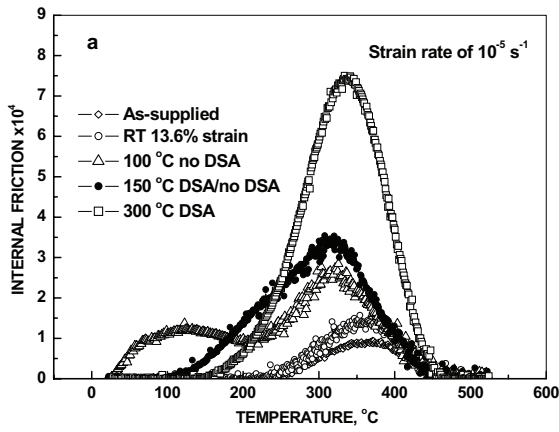

Figure 6. Carbon IF peak evolution with mechanical pre-treatment in Inconel 600 alloy (a) and the amplitude of the IF peak as a function of tensile testing temperature (b).
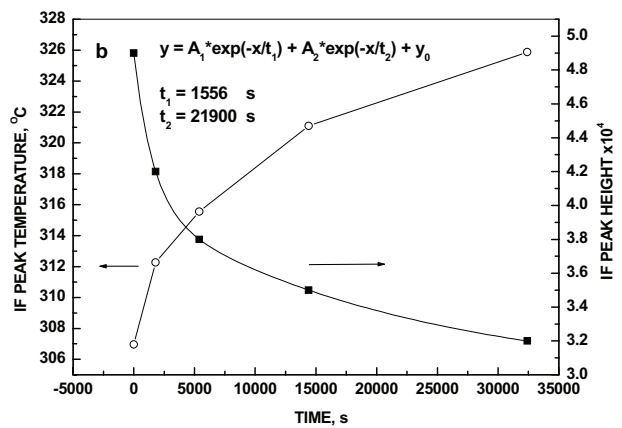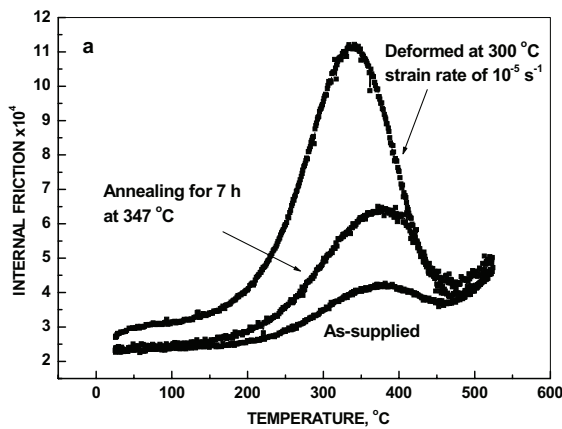

Figure 7. Effect of isothermal annealing on carbon IF peak height (a) and the peak height and temperature position as a function of annealing time at 277 °C in Inconel 600 alloy.

Discussion

Dependencies of the onset of serrations in Inconel 600 and 690 alloys on temperature and strain rate are shown in Fig. 8. The data summarises the appearance of serrations on the stress-strain curves of Inconel 600 and 690 alloys at different strain rates and testing temperatures. In the case of filled data points DSA serrations take place while open ones mean that no serrations were observed. Open and filled grey triangles are data obtained by Mulford and Kocks [13] using compression testing technique. The dotted lines in Fig. 8 represent dependencies of the critical strain rate as a function of testing temperature for DSA occurrence. This dependence is widely used for calculation of enthalpy of DSA occurrence and it can be expressed as

$$\dot{\varepsilon}_c = \dot{\varepsilon}_c^0 \exp\frac{-H}{k_B T},$$

where $\dot{\varepsilon}_c^0$ is a pre-exponential factor, $k_B T$ is temperature in energy units and H is representing the apparent enthalpy of the DSA occurrence. The enthalpies for the onset of DSA calculated from the doted lines in Fig. 8 are about 1.65 eV for both Inconel alloys, but the boundary for Inconel 600 alloy is at lower temperatures as compared to that of Inconel 690 alloy. These enthalpies are in good agreement with the enthalpy value of carbon diffusion in FCC lattice of Inconel 600 alloy calculated from the activation parameters of the carbon IF peak, 1.76 ± 0.06 eV. The evidence of good correspondence of the activation energy values for the onset of DSA serrations to the enthalpy of carbon diffusion value obtained by IF method allows to assume that diffusion redistribution of carbon occurs during plastic deformation in Inconel 600 alloy and probably in Inconel 690 alloy, too. Another fact supporting this evidence comes from the comparison of Fourier analysis results and characteristic times of

short term component of the IF peak decay with annealing time. Average times between pulses of A type serrations are 1.8 ks for Inconel 600 alloy and 1.7 ks for Inconel 690 alloy which correspond to the characteristic time of 1.5 ks for decrease of internal friction peak height for Inconel 600 alloy.

The comparison of the results obtained for the onset of DSA serrations as a function temperature and strain rate with the results of Mulford and Kocks [13] shows that the value of the activation energy for the onset of serrations calculated from their data is about 0.92 eV, which is smaller than the value of the present study and the boundaries of the present study are situated at lower temperatures. The same observation can be made if the results of present study are compared to the range of DSA occurrence in AISI 316 NG stainless steel [9, 10]. The activation energy was obtained in the same way in [17] for Inconel 718SPF alloy. In this study apparent activation energies for the onset of type A and B serrations were in the range of $1 - 1.4$ eV, which correspond well to the present results. In [17] it was suggested that type A and B serrated flow results from the diffusion of an interstitial solute, most likely carbon.

One of the key parameters for classifying Inconel 600 products based on their susceptibility to IGSCC is carbon content and its distribution between solution and carbides. The beneficial effects of carbon in solution on the resistance to IGSCC have been discussed in [20-22]. The influence of carbon was attributed to the improvement of the creep resistance by pinning of the mobile dislocations by carbon atoms and by delaying the recovery process of climb at the grain boundary thereby inhibiting grain boundary sliding and cavitation, thus decreasing the creep rate. Pronounced serrated flow behavior was observed for the carbon containing alloys in argon and PWR primary water indicating strong carbon-dislocation interactions [21]. Increase in the creep rate in the primary water as compared to argon in carbon containing alloys was proposed to be due to hydrogen unpinning dislocations and increasing their mobility based on hydrogen-enhanced localized plasticity models. If IGSCC crack growth is controlled by low temperature time-dependent creep deformation, the environmental effects have to be considered in addition to DSA effects for understanding conditions in the crack tip plastic zone. At the crack tip, oxidation reactions inject vacancies into the plastic zone and hydrogen uptake is also known to increase the local vacancy concentration [23]. Thus, metal vacancies at the crack tip plastic zone are most probably the key factors explaining the crack growth and controlling the crack tip strain rate, while DSA inhibits the plastic strain inside the plastic zone further away from the crack tip. Injected vacancies increase the mobility of dislocations, facilitate dislocation reactions and increase stress relaxation at the crack tip. It can be expected that at the crack tip the environmental effects of oxidation and hydrogen uptake reverse and completely eliminate the effects of carbon in solution and concentrate strain and strain rate close to the SCC crack tip. Thus, the effect of environmental reactions at the SCC crack tip is to unpin dislocations from their carbon/solute atmospheres, lower the activation energy and increase the rate sensitivity of dislocation glide. DSA has just the opposite effects further away from the crack tip: slow moving dislocations become pinned by solute atmospheres and new dislocations are generated to maintain the strain rate, which results in an increase in the dislocation density and the flow stress. On the same time solute atmospheres
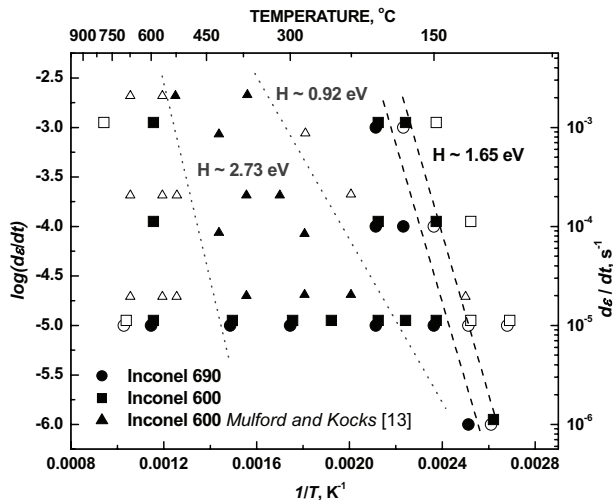

Figure 8. Dependence of the DSA serration appearance on temperature and strain rate for Inconel 600 and 690 alloys shown by squares and circles, respectively. Data points shown by triangles were obtained in [13]. Filled data points correspond to strain rate and temperature values at which the DSA serrations occur on stress-strain curves and open points correspond to smooth flow. The dotted lines are the boundaries for the onset (or disappearance) of serrations.

restrict dislocation cross-slip and climb, which favors planar slip, which again increases the flow stress. These hardening effects induce increasing stress concentration at the crack tip by preventing the stress relaxation inside the plastic zone, which localizes the strain to the crack tip and increases the crack growth rate. An alternative effect of DSA on the reduction of the IGSCC resistance of Inconel 600 alloy can be caused by weakening of the grain boundaries due to the depletion of carbon. It was shown by IF measurements that a remarkable increase of carbon content in solid solution follows DSA occurrence (increase of carbon IF peak in DSA conditions), which means that the plastic flow localization induced by DSA results in carbon escape from grain boundaries to solid solution. The second component of the carbon IF peak decay after DSA (Fig. 7 b), which has characteristic time of 21.9 ks, can correspond to segregation of carbon back to grain boundaries from about 5 μm distance.

The good IGSCC resistance and DSA behavior of Alloy 690 need further considerations, since the carbon solubility in it is markedly lower than that in Alloy 600 [22]. The DSA behavior in both alloys was observed to be similar. However, the higher Cr content of Alloy 690 substantially increases its creep resistance. Chromium alloying reduces the stacking fault energy of the alloy, which may be the reason for the higher creep resistance by inhibited dislocation climb and cross-slip. These positive effects of Cr are even more pronounced than those of carbon, even though the final annealing temperature, i.e. the amount of carbon in solution, is known to have a considerable influence on the IGSCC crack initiation time in Alloy 600. Based on the IF results Cr alloying seems to have some additional effects on carbon solubility and distribution in these alloys, since in Alloy 690 no carbon IF peak was observed after any thermomechanical treatment, which needs further clarification. Additionally, higher Cr content will affect the oxidation reactions controlling vacancy injection and hydrogen uptake in the material, which play key role in strain localization and subsequent crack initiation.

Acknowledgements

Conclusions

The temperature range for appearance of DSA phenomenon in Inconel 600 and 690 alloys increases with decreasing strain rate and at strain rate of 10^{-5} s^{-1} DSA is observed in the temperature range of 150 ... 600 ^{o}C.

No strong effects on mechanical properties caused by DSA were observed.

The activation energy values for the onset of DSA serrations are the same for both Inconel alloys and its value was estimated to be 1.65 eV. This value corresponds well to the enthalpy of carbon diffusion in Inconel 600 alloy obtained by IF method, 1.76 ± 0.06 eV.

In spite of the fact that the value of the activation energy for DSA onset in Inconel alloys is higher than that for AISI 316NG austenitic stainless steel, DSA in Inconel 600 and 690 alloys begins at lower temperatures.

Free carbon induces an internal friction (IF) peak in Inconel 600 alloy at about 350 ^{o}C, while in Inconel 690 alloy carbon IF peak is not detected after any thermomechanical treatment.

Amplitude of the carbon IF peak is markedly increased if Inconel 600 alloy is deformed in the DSA conditions. This effect is probably caused by free carbon enriched submicroscopic zones forming in Inconel 600 alloy during DSA and escape of carbon from grain boundaries.

References

1. H. Hänninen, et al., "Effects of Dynamic Strain Aging on Environment-Assisted Cracking of Low Alloy Pressure Vessel and Piping Steels," *Proc. of 10th International Conference on Environmental Degradation of Materials in Nuclear Power Systems - Water Reactors, Nevada, USA, 5 - 9 August 2001, ANS; NACE; TMS* (2001), 12 p.

2. K. Bhanu Sankara Rao, et al., "Serrated Flow and Deformation Substructure at Room Temperature in Inconel 718 Superalloy During Strain Controlled Fatigue," *Scr. Met. et Mater.*, 32 (1995), 493-498.

3. A.A. Marengo, J.E. Perez Ipiña, "Pressure Vessel Steel Fracture Toughness in the Regime from Room Temperature to 400 ^{o}C," *Nuclear Engineering and Design,* 167 (1996), 215-222.

4. R. Mohan, C. Marschall, "Cracking Instabilities in a Low-Carbon Steel Susceptible to Dynamic Strain Aging," *Acta Mater.*, 46 (1998), 1933-1948.

5. S. Hereñú, I. Alvarez-Armas, A.F. Armas, "The Influence of Dynamic Strain Aging on the Low Cycle Fatigue of Duplex Stainless Steel," *Scr. Mat.,* 45 (2001), 739-745.

6. I.S. Kim, S.S. Kang, "Dynamic Strain Aging in SA508-Class 3 Pressure Vessel Steel," *Int. J. Pres. Ves. & Piping,* 62 (1995), 123-129.

7. L.H. de Almeida, P.R.O. Emygdio, "Activation Energy Calculation and Dynamic Strain Aging in Austenitic Stainless Steel," *Scr. Met. et Mater.*, 31 (1994), 505-510.

8. D.W. Kim, W.-S. Ryu, J.H. Hong, S.-K. Choi, "Effect of Nitrogen on the Dynamic Strain Aging Behaviour of Type 316L Stainless Steel," *J. Mater. Sci.*, 33 (1998), 675-679.

9. M. Ivanchenko, U. Ehrnstén, V. Nevdacha, Y. Yagodzinskyy and H. Hänninen, "Dynamic Strain Ageing of Nitrogen-alloyed AISI 316L Stainless Steel," *Proceedings of the 7th International Conference on High Nitrogen Steels 2004, Ostend, Belgium, September 19-22* (2004), 641 - 649.

10. U. Ehrnstén, M. Ivanchenko, V. Nevdacha, Y. Yagodzinskyy, A. Toivonen, H. Hänninen, "Dynamic Strain Ageing of Deformed Nitrogen-alloyed AISI 316L Stainless Steel," *Proceedings of Eurocorr 2004, Nice, France, 13-16.9* (2004), Event No. 226, 10 p.

11.   Seong-Gu Hong, Soon-Bok Lee, "The Tensile and Low-Cycle Fatigue Behavior of Cold Worked 316L Stainless Steel: Influence of Dynamic Strain Aging," *International Journal of Fatigue,* 26 (2004), 899-910.

12.   Seong-Gu Hong, Soon-Bok Lee, "Mechanism of Dynamic Strain Aging and Characterization of its Effect on the Low-Cycle Fatigue Behaviour in Type 316L Stainless Steel," *Journal of Nuclear Materials,* 340 (2005), 307-314.

13.   R.A. Mulford and U.F. Kocks, "New Observations on the Mechanisms of Dynamic Strain Aging and of Jerky Flow," *Acta Metall.*, 27 (1979), 1125-1134.

14.   A. Kimura and H.K. Birnbaum, "Anomalous Strain Rate Dependence of the Serrated Flow in Ni-H and Ni-C-H Alloys," *Acta Metall.,* 38 (1990), 1343-1348.

15.   Y. Nakada and A. S. Keh, "Serrated Flow in Ni-C Alloys," *Acta Metall. Mater.*, 18 (1970), 437-443.

16.   W. Chen, M.C. Chaturvedi, "On the Mechanism of Serrated Deformation in Aged Inconel 718," *Materials Science and Engineering*, A229 (1997), 163-168.

17.   C.L. Hale, W.S. Rollings, M.L. Weaver, "Activation Energy Calculations for Discontinuous Yielding in Inconel 718SPF," *Materials Science and Engineering*, A300 (2001), 153-164.

18.   L. Fournier, D. Delafosse, T. Magnin, "Oxidation Induced Intergranular Cracking and Portevin - Le Chatelier Effect in Nickel Base Superalloy 718," *Materials Science and Engineering*, A316 (2001), 166-173.

19.   P. Aaltonen, et al., "Study of Snoek-type Relaxation in Hydrogenated Inconel 600," *Philosophical Magazine*, A78 (1998), 979-994.

20.   J.L. Hertzberg and G.S. Was, "The Effect of Carbon on Grain Boundary Diffusivity in Ni-16Cr-9Fe Alloys," *Scr. Met. et Mater.*, 33 (1995), 1193-1199.

21.   J.L. Hertzberg, G.S. Was, "Isolation of Carbon and Grain Boundary Carbide Effects on the Creep and Intergranular Stress Corrosion Cracking Behavior of Ni-16Cr-9Fe-xC Alloys in 360 °C Primary Water," *Met. Trans.*, 29A (1998), 1035-1046.

22.   K. Stiller, J.-O. Nilsson, K. Norring, "Structure, Chemistry, and Stress Corrosion Cracking of Grain Boundaries in Alloys 600 and 690," *Met. Trans.*, 27A (1996), 327-341.

23.   P. Aaltonen, et al., "Vacancy-Creep Model for EAC of Metallic Materials in High Temperature Water," *Corrosion 96, NACE, 25-28.3.1996, Colorado, Denver, USA*, Paper No. 81, 12 p.